International Journal of Fracture **119/120:** 487–499, 2003.

Mechanical properties and fracture toughness of organo-silicate glass (OSG) low-*k* dielectric thin films for microelectronic applications

J.B. VELLA[1], I.S. ADHIHETTY[1], K. JUNKER[2] and A.A. VOLINSKY[1]
[1]*Motorola, DigitalDNA™ Labs, Process and Materials Characterization Lab, Tempe, AZ 85284, U.S.A. (E-mail: joseph.vella@motorola.com)*
[2]*Motorola, Digital DNA™ Labs, Advanced Product Research and Development Lab, Austin, TX 78721, U.S.A.*

Abstract. The integration of chemical vapor deposited organo-silicate glass (OSG) interlayer dielectrics (ILD) has challenged the IC industry to formulate new methods of metrology and characterization. The impact of nanoindentation to understand and screen for integrated circuit failure mechanisms that are mainly predicated upon OSG nano-porosity is discussed. Failure modes include poor mechanical strength, low material stiffness, and brittle fracture due to low cohesive and adhesive fracture toughness, a particular danger during chemical-mechanical polishing (CMP). By developing a methodology to predict failure modes, we are able to screen multiple candidate low-*k* materials. Nanoindentation measurements of elastic modulus, hardness, and fracture toughness and what they reveal about OSG porosity are discussed.

Key words: Adhesion, fracture toughness, low-*k* dielectrics, mechanical properties, thin films.

1. Introduction

As the IC industry pushes miniaturization limits beyond the 0.13 μm technology node, novel interline dielectric materials, so called low-*k* materials ($k < 4$), are targeted to completely replace PE-CVD deposited SiO_2 to prevent capacitive crosstalk and interline leakage. These materials are commonly very porous ($> 30\%$) and somewhat organic in nature, which necessarily incur compromises in either the thermal or mechanical integrity with respect to traditional SiO_2 dielectrics.

A viable low-*k* dielectric material must survive a litany of processing steps that include dual-damascene lithography, etching, stripping and cleaning processes, CMP, and device packaging. The reliability of devices containing these multi-layer dual-damascene stacks depends heavily on the mechanical stability of the dielectric, as this is the material and structural template in which the IC functionality is laid. For instance, since the dual-damascene stack is exposed to high shear stresses during the CMP process, any flaws at the interfaces or in the low-*k* film itself can lead to crack initiation and long-term reliability problems.

There are two major classes of low-*k* materials; porous silicates also known as organo-silicate glasses (OSG) and polymeric films. The ceramic nature of OSG films gives the material a high degree of thermal stability but low fracture toughness, further compromised by the porous nature of the film. Polymer low-*k* films, generally spin-on deposited, meanwhile generally have high fracture toughnesses, yet poor thermal as well as mechanical stiffness properties. In this paper we address the characterization of OSG films.

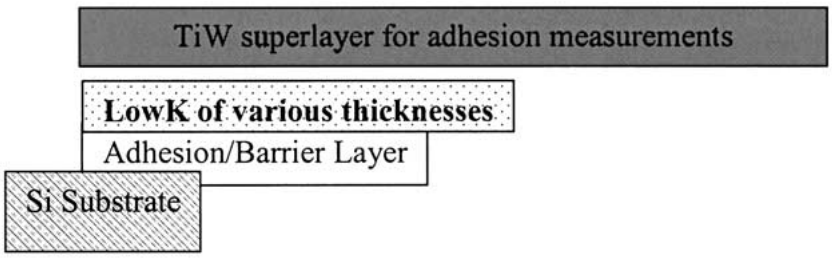

Figure 1. Schematic of a typical low-K test structure.

Nanoindentation has emerged as a critical technique for material evaluation in the IC industry because of the special problems that thin or sub-micron films present. Thin films often exhibit far higher yield strengths than their bulk counterparts due to several factors including nanostructured grains in crystalline films, the fact that film is attached to a substrate, and the length scale restriction in the z-dimension for dislocation movement (Hardwick, 1987; Nix, 1998). Due to typically high yield strengths, thin films can support very high as-deposited residual stresses (Ohring, 1992). These residual stresses can be relieved later during processing or in the actual device operation through plastic deformation, thin film fracture, or interfacial delamination. Elastic and plastic properties of thin films have been measured by tensile testing of freestanding films (Hoffman, 1966; Read and Dally, 1993) and by the microbeam cantilever deflection technique (Nix, 1989; Baker and Nix, 1994; Weihs et al., 1998). However the most straightforward way is by means of nanoindentation, since no special sample preparation is required and tests can be performed quickly and inexpensively (Oliver, 1986; Doerner and Nix, 1986; Oliver and Pharr, 1992). To evaluate the device mechanical stability four material properties of the device components are important: elastic modulus, hardness, interfacial adhesion, and film fracture toughness.

Mechanical properties such as hardness and elastic modulus, E, have become almost routine metrics for thin films using nanoindentation. During the measurement a sharp pyramidal diamond indenter, such as a Berkovich indenter, is forced into the material of interest while continuously recording both the force and the indentation depth. Mechanical properties are measured by either analyzing the load-displacement profile or by measuring the material response to a frequency modulated load oscillation. Since the depth resolution is on the order of nanometers, it is possible to measure these properties in even very thin (> 100 nm) films.

Indentation can also be used to measure thin film adhesion (Marshall and Evans, 1984; Vlassak et al., 1997; Kreise and Gerberich, 1999; Vella et al., 2000; Volinsky et al., 2002a), where the mechanical energy release rate, G, or practical work of adhesion is calculated based on the size of an indentation induced delamination. Furthermore fracture properties such as fracture toughness can be derived from crack lengths of film fracture generated by tip facet edges (Pharr et al., 1993; Harding et al., 1995).

2. Experiment

A series of OSG low-k films underwent a battery of nanoindentation tests to measure elastic modulus, hardness, adhesion strength, and fracture toughness. This paper details the nature of those measurements as well as some of their results. These films were CVD deposited on barrier metal coated $\langle 100 \rangle$ silicon wafers to thicknesses ranging from 50 nm to 3000 nm.

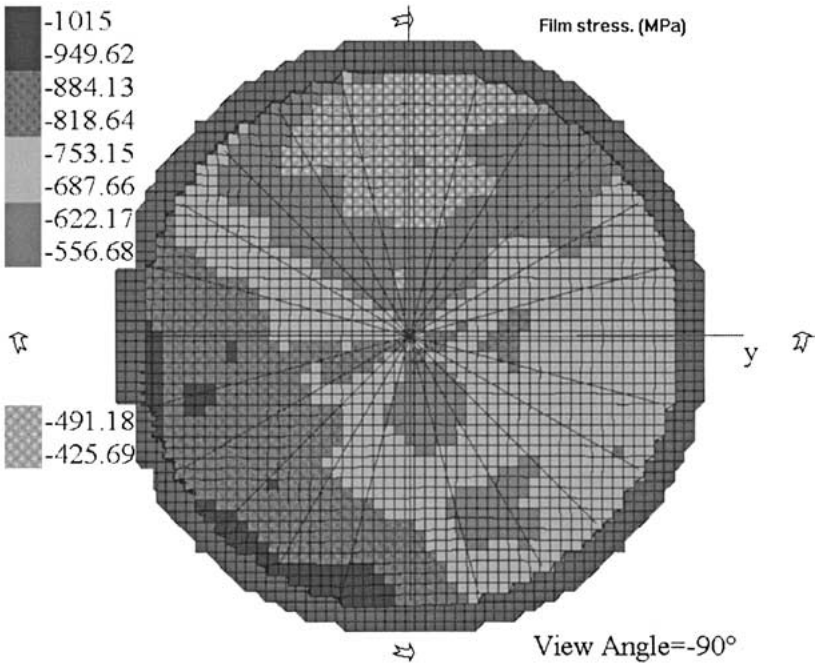

Figure 2. Residual stress map of a 1 μm thick TiW superlayer.

A schematic of a typical low-k test structure is shown in Figure 1. As-deposited or residual stress measurements were made for all low-k film thicknesses. Several samples were also coated with an RF sputter-deposited TiW superlayer to a thickness of 1 μm for the interfacial adhesion measurements. The average residual stress in the superlayer was on the order of 1 GPa measured, like the low-k as deposited stress measurements, with the wafer curvature technique employing Stoney's equation (Stoney, 1909) modified for the two-dimentional case:

$$\sigma_R = \frac{E_s}{1-\nu_s}\frac{h_s^2}{6h_f R_1}\left[1+\left[\frac{\nu}{1+\nu}\right]\left[\frac{R_1}{R_2}-1\right]\right], \tag{1}$$

where E_s is the elastic modulus of the substrate, and ν_s is the Poisson's ratio of the substrate, h_s is the substrate thickness, h_f is the film thickness, and R_1 and R_2 are the radii of curvature in the $x-z$ and $y-z$ planes respectively. Substrate curvature radii after each thin film deposition step were measured accurately with laser deflection and optical lever cantilever beam techniques. This allows constructing a stress map over the whole wafer. Figure 2 shows a typical stress map for a 1 μm TiW film on Si.

Elastic modulus and hardness of different low-k materials from different vendors were measured by nanoindentation using both NanoIndenter XP™ and Hysitron Triboindenter™. Studies using the NanoIndenter XP™ were carried out using a frequency and tip displacement modulated measurement; 75 Hz and 1 nm respectively. The dynamic response of the material, or phase angle δ is used to measure the hardness and modulus (Oliver and Pharr, 1992). For the measurements made with the Hysitron Triboindenter™ the initial slope of the unloading curve is used to extract mechanical properties from the individual load-displacement curves.

Adhesion measurements were performed using the NanoIndenter XP™ and a conical diamond tip with a 1 μm tip radius. Indentation loads of 100–600 mN were required to cause

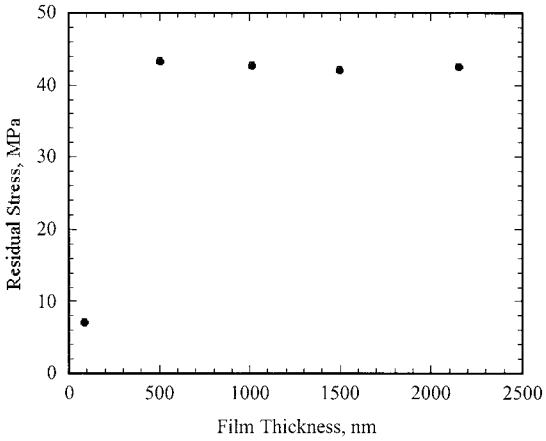

Figure 3. Low-k films residual stress as a function of the thin film thickness.

delamination blisters to form. Satisfactory blisters are those whose radius exceeded at least twice the estimated plastic zone around the indent.

Adhesion measurements of this type also require knowledge of the as-deposited stress residing in the low-k film that will be released (compressive) or must be overcome (tensile) to initiate delamination. It is interesting to note in Figure 3 the trend of residual stress with film thickness in the OSG process under study. At a critical film thickness of 3 μm, spontaneous film cracking is typically observed allowing the relief of residual tensile stress in the film (Volinsky et al., 2002a).

Film fracture toughness measurements were performed using medium load nanoindentation (5–20 mN) with a cube corner indenter. Further discussion of adhesion and fracture toughness measurement techniques is included in the following sections.

3. Low-k films microstructure and mechanical properties

As air has a dielectric constant of unity, one logical solution to reducing the dielectric constant of the ILD without changing the chemical composition is to introduce pores, as is the case with OSG films. However, introducing these pores in a controlled manner with a narrow pore size distribution requires a highly optimized deposition process. For CVD deposited OSG this problem can be solved by introducing terminal methyl groups (-CH_3) that interrupt the Si-O network thus creating nano-pores, each on the order of the volume of a methyl group ($\sim$4 nm). Figure 4 illustrates a molecular dynamics cartoon of a CVD deposition of an OSG film. With the introduction of these methyl groups, the SiO_2 lattice is forced to grow around the inclusion with little or no further bonding to the inclusion. These inclusions compromise the mechanical stability of silica due to a decreased concentration of Si-O bonds as well as an increased propensity for pore and density non-uniformity (Loboda, 2000; Vella et al., 2001).

There are well-documented predictive models of mechanical properties for solid foams as a function of porosity based on the existence of closed cell and open cell pores in the material (Gibson and Ashby, 1988). One of the more widely used models describe how the deformation mechanism is related to material distribution about the cell edge versus the cell face as well as to the relative density of the material. Equations (2)–(4) illustrate trends in elastic modulus, hardness, fracture toughness. The parameter ϕ is the fraction of material on the cell face to

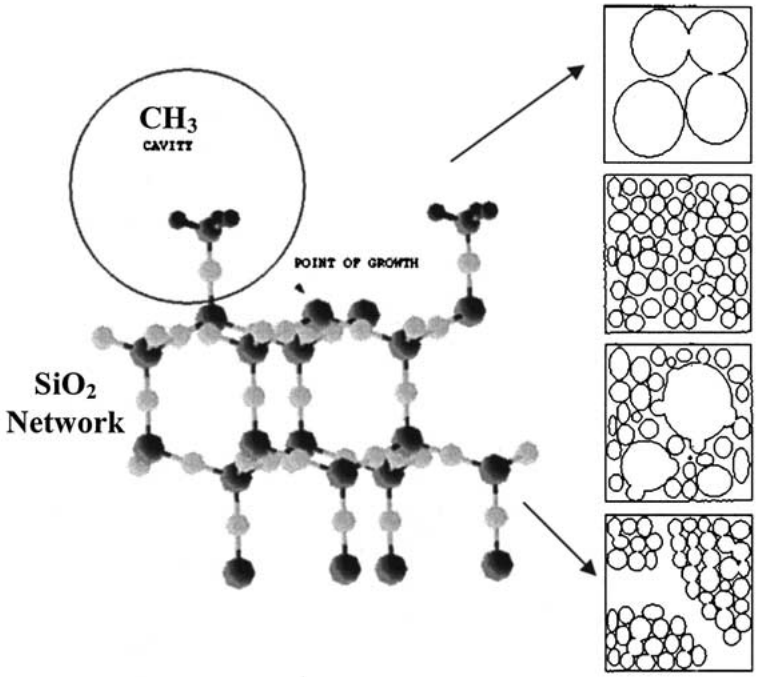

Figure 4. Porosity formation process in a low-K dielectric thin film.

the cell edge. These porosity relations have similar forms for shear modulus, crush strength, and compressive and tensile yield stresses.

$$\frac{E^*}{E_0} = \left(1 - \frac{p^*}{p_0}\right)^2 \text{ open cell; } \frac{E^*}{E_0} = \phi^2 \left(1 - \frac{p^2}{p_0}\right)^2 + (1-\phi)\left(1 - \frac{p^*}{p_0}\right) \text{ closed cell;} \tag{2}$$

$$\begin{aligned} \frac{H^*}{H_0} &= 0.23 \left(\frac{p^*}{p_0}\right)^{3/2} \left(1 + \left(\frac{p^*}{p_0}\right)^{1/2}\right) \text{ open cell;} \\ \frac{H^*}{H_0} &= 0.3 \left(\phi \frac{p^*}{p_0}\right)^{3/2} + (1-\phi)\left(1 - \frac{p^*}{p_0}\right) \text{ closed cell;} \end{aligned} \tag{3}$$

$$\frac{K_{IC}^*}{K_{IC}} = 0.65 \left(1 - \frac{p^*}{p_0}\right)^{3/2} \text{ for open cell; } \frac{K_{IC}^*}{K_{IC}} = \left(1 - \frac{p^*}{p_0}\right)^{3/2} \text{ for closed cell.} \tag{4}$$

As described previously, the nature of the porosity of OSG materials appears to be quite different than other porous materials because of the way that the porosity is generated. Rather than macroscopic pores, open or closed, the pores are created by methyl inclusions on a molecular scale, which cannot be easily discerned even using high resolution TEM seen in Figure 5. These images show what appears to be a diffuse amorphous structure. Distinct pores cannot be discerned *per se*. Such nano-porosity has necessary advantages for IC applications as pores with a diameter greater than 10 nm or so would be deleterious from a mechanical as well as a processing point of view to a dielectric wall less than 130 nm thick. Given the nature of the fundamental differences in porosity in this class of materials as compared to macroscopic porosity, a relaxation of these predictive models is warranted using a more

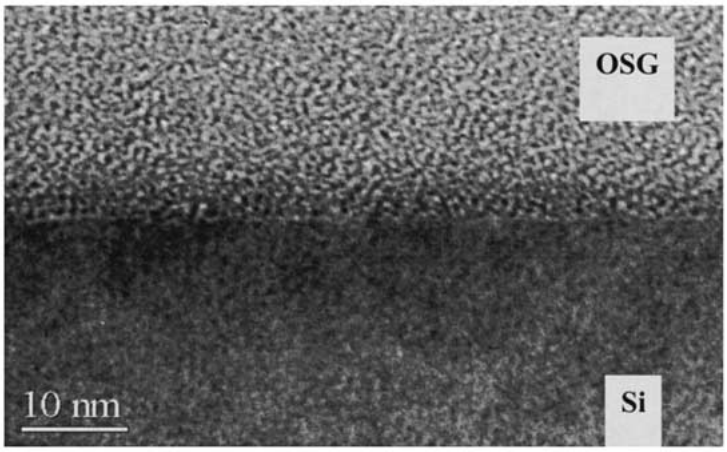

Figure 5. Cross-sectional TEM image of a low-k film on a Si substrate showing nanoporous low-k film structure.

empirical form of these relations shown in Equation (5) with adjustable parameters f and α where X represents the material property being fit (Phani and Niyogi, 1987). This form can be used to fit ceramic and metal foam data whose porous structure may deviate from the discrete open or closed cell forms.

$$\frac{X^*}{X_0} = \alpha \left(1 - \frac{p^*}{p_0}\right)^f \tag{5}$$

The utility of drawing this kind of correlation is threefold. If we conclude that our dielectric character is generated primarily by the porosity of our film, we can anticipate the compromise in mechanical properties that will be incurred when optimizing the dielectric properties. This correlation will also allow the process engineer to rapidly determine the porous and dielectric nature of the film merely via nanoindentation assuming the absence of a radical change in chemistry. An example of such a correlation of elastic modulus is shown in Figure 6. This measure can be strengthened by the cross correlation of hardness and fracture toughness measurements. Presently employed techniques for this measurement such as positron annihilation lifetime spectroscopy (PALS) (Gidley et al., 2000; Kondoh et al., 2001), spectroscopic ellipsometry (Baklanov, 2000; Edwards et al., 2001), or X-ray reflectivity (Lin et al., 2000) can be expensive and/or time consuming. However these techniques remain indispensable, as they are necessary to validate the porosity correlation. And thirdly, it allows nanoindentation to be used as a metrology flag to indicate changes in the CVD process transparent to other techniques that are typically used to measure changes in chemical composition such as X-ray photoelectron spectroscopy.

Typically low-k thin film mechanical properties vary considerably as a function of indentation depth. The profile of elastic modulus and hardness often take the shape of a check mark as a function of depth. A typical indentation profile is shown in Figure 7. The increased modulus at low indentation depths is not well understood although it may be attributed to several factors including an indentation size effect (Pharr and Oliver, 1989), material surface overshoot where the tip may actually have penetrated the material prior to surface detection causing an underestimate in contact area, or correspond to a real change in surface composition. A global minimum is then usually observed in the profile. Convention holds that this point indicates the best estimate of the mechanical properties for the film in the absence of FEM verification.

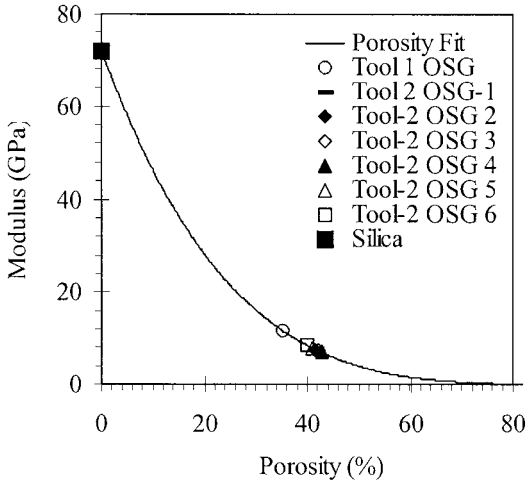

	Modulus (GPa)	Percolation Porosity (%)
Tool 1 OSG	11.7	35.1
Tool 2 OSG-1	7.60	41.4
Tool 2 OSG-2	7.49	41.6
Tool 2 OSG-3	7.24	42.1
Tool 2 OSG-4	6.90	42.8
Tool 2 OSG-5	7.92	40.9
Tool 2 OSG-6	8.32	40.1
Silica	72.00	0.0

Figure 6. Elastic modulus of porous OSG films as a function of porosity for a series of process tools.

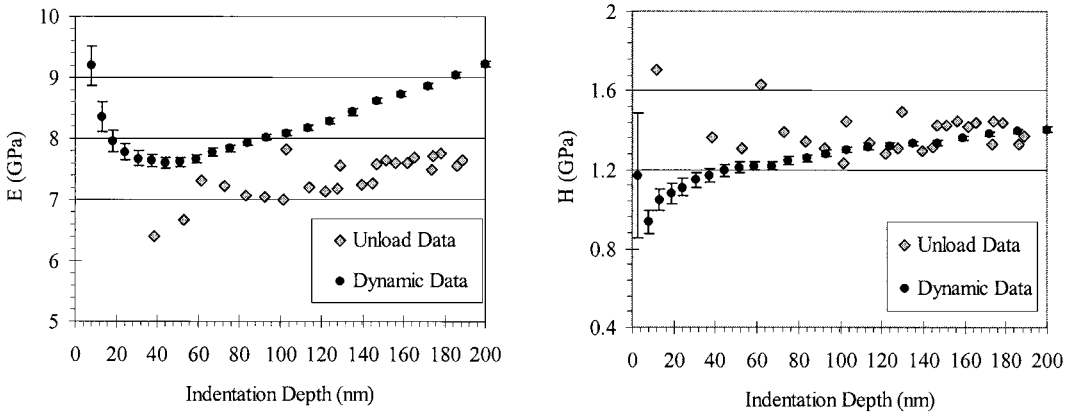

Figure 7. Elastic modulus and hardness profiles of a 1 μm thick low-k dielectric film as a function of indentation depth.

Subsequent to the profile minimum the increase can be attributed to an increasing contribution of the silicon substrate ($E \sim 160$ GPa) on the contact stiffness. Using the minimum of this profile is not foolproof, however, because some films' surface effects may overlap with their substrate effects thereby inflating the minimum point.

According to recent studies at Sematech there appeared to be a correlation between elastic modulus and the films ability to withstand chemical-mechanical polishing. However, because these films' mechanical and fracture properties are intimately linked with their porosity, correlation with CMP failure can also be made with the film hardness or fracture toughness. Figure 8 shows the seemingly linear relationship of hardness and modulus that stems from the variation in porosity of a group of silicate films. The correlation of open, closed, and empirical fits show how the OSG materials under study can be fit to obtain information on the porosity behavior. Using relations (2)–(5) one can back out an estimate of porosity based on the modulus, hardness, of fracture toughness once the correlation has been established. Others have also shown that the fracture toughness measured using the Modified Edge Lift-off test (mELT) technique can be correlated with the dielectric constant (Schaffer et al., 2000).

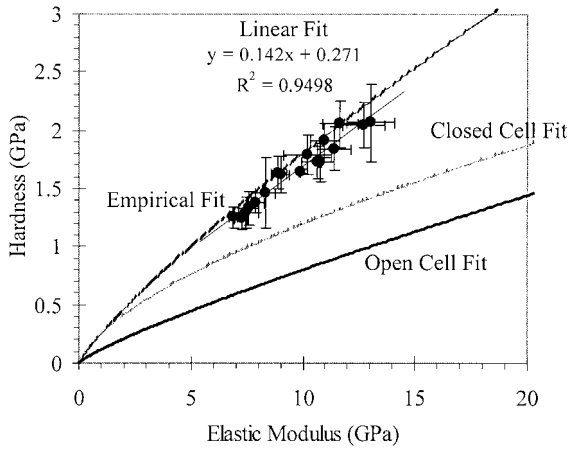

Figure 8. Linear plot of silicate low-*k* dielectric film hardness versus modulus, demonstrating the interrelated mechanical properties.

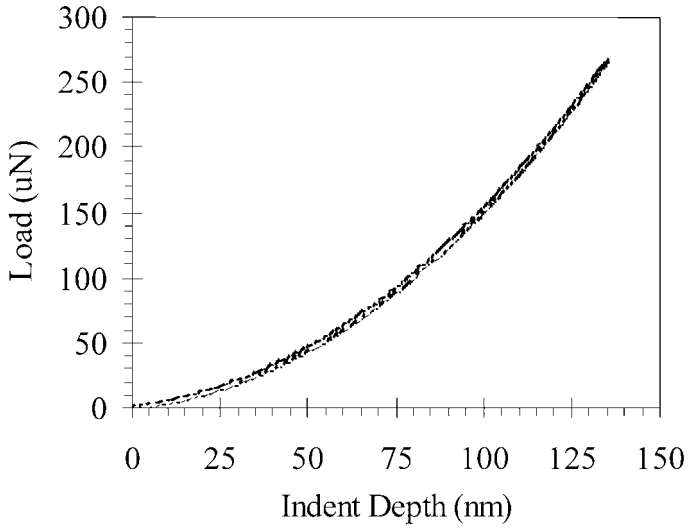

Figure 9. Load-displacement curve for a 1 mm thick OSG low-*K* dielectric film showing no plasticity or permanent deformation.

It is important to note that the OSG films tested in this study were observed to generate purely elastic contacts during nanoindentation. That is, very little or no plasticity was observed in the film at depths where the minimums occurred in the modulus versus displacement profile. A typical load displacement profile curve is seen in Figure 9, which shows no permanent deformation in the low-*k* film. Therefore measurements of both modulus and hardness for these low-*k* films, typically at approximately 10% of the film thickness, appear to be redundant measures of the elastic properties.

4. Low-*k* film fracture

With OSG's high hardness to modulus ratio typical of brittle glasses one may expect low fracture toughness and adhesion values. These properties were measured initially by means

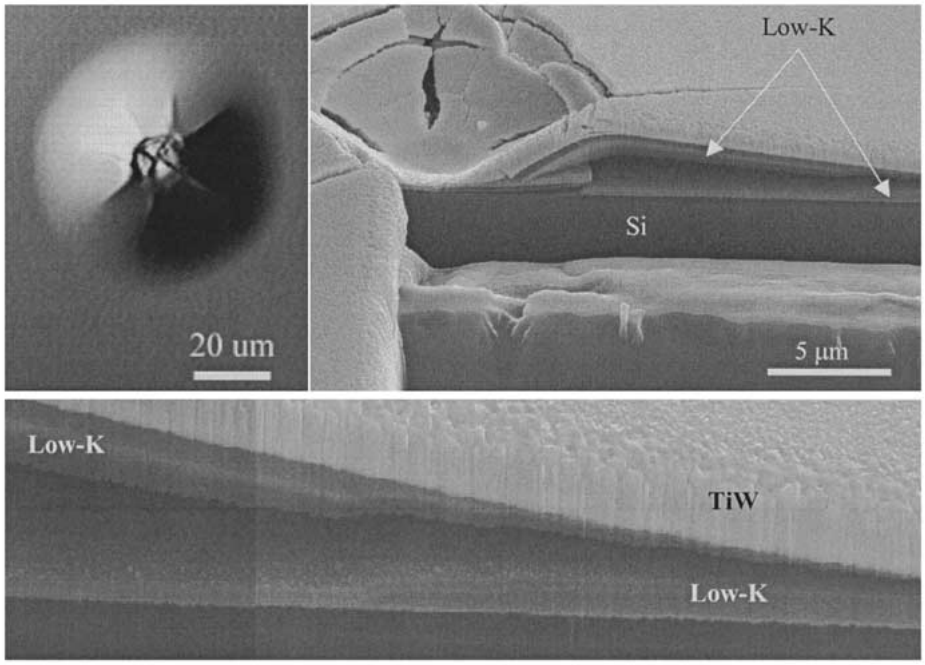

Figure 10. Focussed ion beam cross-section of the superlayer indentation-induced blister showing fracture in the low-K dielectric layer.

of a superlayer indentation technique. Most low modulus films cannot be delaminated by means of regular indentation because these films cannot effectively transfer the indentation stress to the film/substrate interface. Rather the indentation stress is simply absorbed by elastic deformation or relieved by plasticity in the film. To prevent these problems a high modulus, high hardness superlayer, capable of supporting and storing large amounts of elastic energy is deposited on top of the film of interest. Upon indentation the superlayer allows an interfacial crack to form and propagate laterally to relieve the indentation stress as well as the superlayer residual stress. In this way a delamination blister is formed around the indent whose area is used to calculate the strain energy release rate (practical work of adhesion). This technique requires verification of the interfacial crack, which is done by Focused Ion Beam (FIB) cross-sectioning and subsequent Scanning Electron Microscopy (SEM) imaging. Indeed, upon closer analysis of the OSG adhesion blisters it was found that in most cases a cohesive low-k fracture mechanism competes with the adhesive fracture seen in Figure 10. The strain energy release rate that is calculated reflects a combination of cohesive and adhesive fracture events. It is likely that the interface and the OSG material itself have similar fracture toughnesses but have different dependences on phase angle causing the crack tip to kink from an adhesive to a cohesive mode as the blister expands. In our previous study we have estimated 0.2 to 0.8 J m^{-2} for the strain energy release rate in the low-k dielectrics based on the superlayer indentation adhesion measurements (Volinsky et al., 2002a).

Although somewhat more problematic, fracture toughness evaluation can also be quickly carried out using indentation. When a sharp tip such as a cube corner diamond is forced into a bulk sample of brittle material, radial cracking usually occurs after a critical load has been reached, emanating from stress concentrations at the diamond facet edges (Figure 11), which allows one to calculate fracture toughness based on the maximum indentation load and the

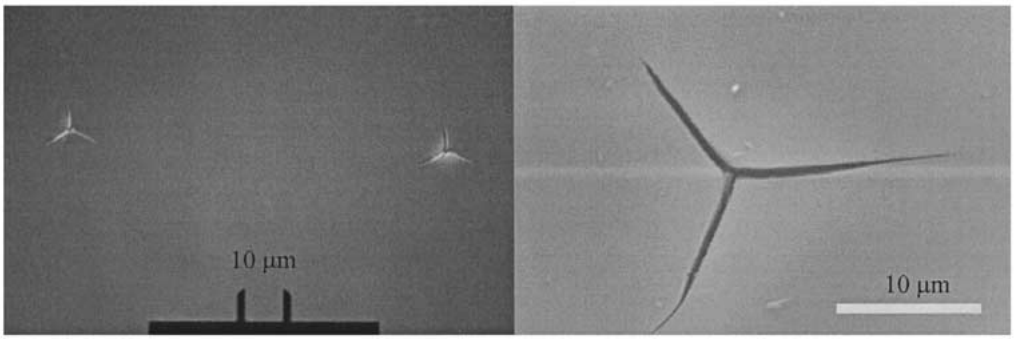

Figure 11. Optical and SEM image of cube-corner indentation-induced fracture in a 1 μm thick OSG low-K dielectric film.

crack length (Lawn and Wilshaw, 1975; Antis et al., 1981; Lawn et al., 1980). The fracture toughness of a bulk brittle material can be estimated based on the maximum indentation depth, $P_{\max}$ and the crack length, c (Harding et al., 1995):

$$K_C = \alpha \left(\frac{E}{H}\right)^{1/2} \left(\frac{P_{\max}}{c^{3/2}}\right) \tag{6}$$

where α is an empirical constant which depends on the geometry of the indenter, E is the elastic modulus, and H is the hardness. This method of analysis in complicated in the case of thin film radial fracture, since typically the film is too thin for the crack to have a halfpenny shape. Furthermore, the stress field created by the indenter is perturbed by the underlying substrate. It was also noted in the previous study that the maximum indentation load scales linearly with the crack length to the 3/2 power, so as a first-order approximation Equation (6) can be used to estimate low-k films fracture toughness (Volinsky et al., 2002). Figure 12 shows how fracture toughness scales with the maximum indentation load. The fracture toughness results in Figure 12 are of the same order of magnitude as presented by He et al. (2002) measured by means of the channel cracking test (Xia et al., 2000). However the impact of the substrate and micron-scale film thickness is clear from the fracture toughness dependence on indentation load. That is, progressively deeper indents incur greater perturbation of the stress field and half-penny shape of the crack thus retarding crack growth. Therefore it would be expected that optimization of the indentation load for a given film of a given thickness is necessary.

Another important method of estimating the film fracture toughness can be found in the observed spontaneous film shattering when the film reaches a critical thickness. Typically at films thicknesses of greater than 3 μm OSG films shatter due to the residual stress relief as can be seen in Figure 13. The low-K dielectric film tensile residual stress is approaching 44 MPa starting from the 0.5 μm film thickness (Figure 3), so one can estimate the strain energy release rate, G for this material following Hutchinson and Suo (1992) analysis:

$$G = Z\frac{(1-\nu_f^2)\sigma_R^2 h}{E_f} \tag{7}$$

where σ_R is the residual stress, h is the film thickness, and E_f is the film elastic modulus, and Z ranges from $\frac{1}{2}$ to 4, depending on the sample geometry and the residual stress sign. In the case of 44 MPa tensile residual stress ($Z = \frac{1}{2}$) for a 3 μm critical film thickness, one

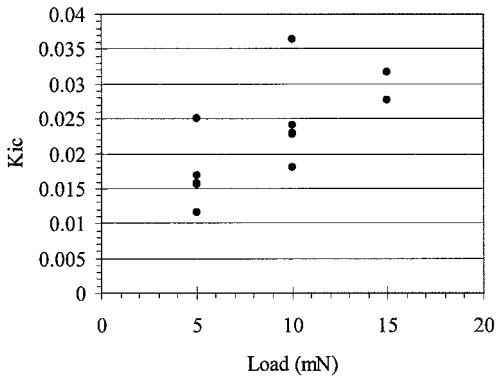

Figure 12. Low-*k* dielectric fracture toughness as a function of the maximum indentation load.

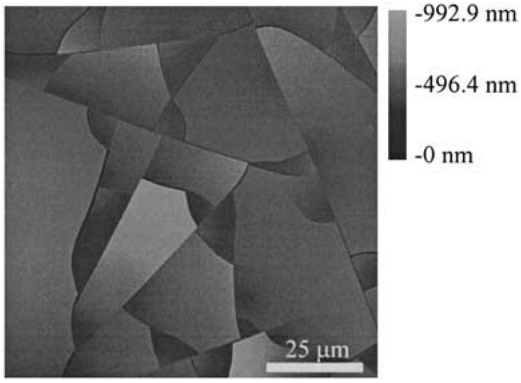

Figure 13. Atomic Force Microscopy image of spontaneous fracture of OSG film driven by as-deposited tensile stress.

would get 0.256 J m^{-2} energy release rate for a 9 GPa elastic modulus, corresponding to about 0.054 MPa $m^{1/2}$. A simple analysis like this can provide realistic upper estimates of the thin film adhesion/toughness. Based on the knowledge of the residual stress and the film thickness, one can come up with a fracture criterion just due to the residual stress:

$$K_C \leq \sigma_R \sqrt{Zh} \tag{8}$$

Equation (8) is similar to a definition of K, except here the film thickness is used instead of the flaw size, or the crack length (Marshall et al., 1982). Work on the impact of OSG porosity on fracture toughness is the subject of ongoing work.

5. Conclusions

This paper describes a methodology to use nanoindentation to measure modulus, hardness, and adhesion, and fracture toughness of various classes of low-*k* materials. These properties are used to predict mechanical reliability of advanced IC devices. By correlating mechanical properties to mechanical reliability we have an effective approach to screening new dielectric materials as well as accessing a porosity metric quickly and inexpensively through nanoindentation.

Acknowledgements

The authors would like to acknowledge the support of the Motorola research engineers Cindy Goldberg and Nicole Grove for matierials deposition, Ginger Edwards for spectroscopic ellipsometry measurements, Bruce Xie and Marti Erikson for TEM analysis, Xiang-Dong Wang for atomic force microscopy measurements, and Anatoli Korkin for microstructure simulations. For valuable discussions we would like to thank Professor W.W. Gerberich.

References

Anstis, G.R., Chantikol P., Lawn, B.R. and Marshall, D.B. (1981). A critical evaluation of indentation techniques for measuring fracture toughness: I. Direct crack measurements. *Journal of the American Ceramics Society* **64**(9), 533–538.

Baker, S.P. and Nix, W.D. (1994). Mechanical properties of compositionally modulated Au-Ni thin films: nanoindentation and microcantilever deflection experiments. *Journal of Materials Research* **9**(12), 3131–3152.

Baklanov, M.R., Moglinikov, K.P., Polovinkin, V.G. and Dultzev, F.N. (2000). Determination of pore size distribution in thin films by ellipsometric porosimetry. *Journal Vacuum Science and Technology* **B18**(3), 1385–1391.

Doerner, M. and Nix, W.D. (1986). A method for interpreting the data from depth-sensing indentation instruments. *Journal of Materials Research* **1**, 601–609.

Edwards, N.V. Vella, J.B. Xie, Q. Zollner, S. Werho, D. Liu, R. Adhihetty, I. Vires, J. and Junker, K. (2001). Spectroscopic ellipsometry as a potential in-line optical metrology tool for relative porosity measurements of low-K dielectric films. *Materials Research Society Proceedings* **695**, L6.25.

Gibson, L.J. and Ashby, M.F. (1988). *Cellular Solids: Structure and Properties*. Pergamon Press, New York.

Gidley, D.W., Frieze, W.E., Dull, T.L., Yee, A.F., Nguyen, C.V. and Yoon, D.Y. (2000). Determination of pore-size distribution in low-dielectric thin films. *Applied Physics Letters* **76**(10), 1282.

Harding, D., Oliver, W. and Pharr, G. (1995). Cracking during nanoindentation and its use in the measurement of fracture toughness. *Materials Research Society Symposium Proceedings* **356**, 663–668.

Hardwick, D.A. (1987). The mechanical properties of thin films: a review. *Thin Solid Films* **154**, 109–124.

He, J. Guanghai, X. Andideh, E. and Maiz, J. (2002). *Fracture Behavior of Low-k Thin Films*. Presented at the 14th US National Congress of Theoretical and Applied Mechanics: Mechanics Of Thin Films And Other Small Structures Symposium organized by Z. Suo, 8 June 2002, Virginia Tech, Blacksburg, VA 14/ 23-2.

Hoffman, R.W. (1966) In: *Physics of Thin Films* (edited by Hass, G. and Thun, R.E.), Vol. 3, Academic Press, New York.

Hutchinson, J. and Suo, Z. (1992). Mixed-mode cracking in layered materials. *Advances in Applied Mechanics* **29**, 63.

Kondoh, E., Baklanov, M. R., Lin, E., Gidley, D. and Nakashima, A. (2001). Comparative study of pore size of low-dielectric-constant porous spin-on-glass films using different methods of nondestructive instrumentation. *Japanese Journal of Applied Physics, Part 2 (Letters)* **40**, L323–L326.

Kriese, M.D. and Gerberich, W.W. (1999). Quantitative adhesion measures of multilayer films. Part I. Indentation mechanics. *Journal Materials Research* **14**(7), 3007–3018.

Lawn, B.R. and Wilshaw, R. (1975). Indentation fracture: principles and applications. *Journal of Materials Science* **10**, 1049–1081.

Lawn, B.R., Evans, A.G. and Marshall, D.B. (2000). Elastic/plastic indentation damage in ceramics: the median/radial crack system. *Journal of the American Ceramics Society* **63**(9–10), 574–581.

Lin, E.K., Wu, W-L., Jin, C. and Wetzel, J.T. (2000). Structure and property characterization of porous low-k dielectric constant thin films using X-ray reflectivity and small angle neutron scattering. *Materials Research Society Symposium Proceedings* **612**, D411–D418.

Loboda, M.J. (2000). New solutions for intermetal dielectrics using trimethylsilane-based PECVD processes. *Microelectronic Engineering* **50**(1–4), 15–23.

Marshall, D.B. and Evans, A.G. (1984). Measurement of adherance of residually stressed thin films by indentation: I. Mechanics of interface delamination. *Journal of Applied Physics* **56**(10), 2632–2638.

Marshall, D.B., Lawn, B.R. and Evans, A.G. (1982). Elastic/plastic indentation damage in ceramics: the lateral crack system. *Journal of the American Ceramic Society* **65**(11) 561–566.

Nix, W.D. (1989). Mechanical properties of thin films. *Metallurgical Transactions A – Physical Metallurgy & Materials Science* **20A**(11), 2217–2245.

Nix, W.D. (1998). Yielding and strain hardening of thin metal films on substrates. *Scripta Materialia* **39**(4–5), 545–554.

Ohring, M. (1992). *The Materials Science of Thin Films*, Academic Press, New York, 403.

Oliver, W.C. (1986). Measurement of Thin Film Mechanical Properties using Nanoindentation. *MRS Bull.* **XI**(5), 15.

Oliver, W.C. and Pharr, G.M. (1992). Improved technique for determining hardness and elastic modulus using load and displacement sensing indentation experiments. *Journal of Materials Research* **7**(6) 1564–1580.

Phani, K.K. and Niyogi, S.K. (1987). Young's modulus of porous brittle solids. *Journal of Materials Science* **22**, 257.

Pharr, G.M. and Oliver, W.C. (1989). Nanoindentation of silver-relations between hardness and dislocation structure. *Journal of Materials Research* **4**(1), 94–101.

Pharr, G.M., Harding, D.S. and Oliver, W.C. (1993). In: *Mechanical Properties and Deformation Behavior of Materials Having Ultra-Fine Microstructures* (edited by Nastasi, M. et al.), Kluwer Academic Press, Dordrecht, HOlland, 449–461.

Read, D.T. and Dally, J.W. (1993). New method for measuring the strength and ductility of thin films. *Journal of Materials Research* **8**(7), 1542–1549.

Schaffer, E.O. II, Howard, K.E., Mills, M.E., and Townsend, P.H. (2000). On the Mechanical Integrity of Ultra Low Load Dielectric Constant Materials for Use in ULSI BEOL Structures. *Materials Research Society Symposium Proceedings* **612**, D1.1.1.

Stoney, G.G. (1909). *Proceedings of the Royal Society of London* **A82**, 72.

Vella, J.B. Die, Q. Edwards, N.V. Kulak, J. and Junker, K.H. (2001). Mechanical properties and porosity of oregano-silicate glass (OSG) low-*k* dielectric films. *Materials Research Society Proceedings* **695**, L6.25.

Vella, J.B. Volinsky, A.A. Adhihetty, I.S. and Gerberich, W.W. (2002). *Materials Research Society Symposium Proceedings* **716**, B12.12.

Vella, J.B. Smith, S.M. Volinsky, A.A. and Adhihetty, I.S. (2000). Adhesion quantification of post-CMP copper to amorphous SiN passivation by nanoindentation. *Materials Research Society Symposium – Proceedings* **649**, Q6.1.1–Q6.1.6.

Vlassak, J.J. Drory, M.D. and Nix, W.D. (1997). Simple technique for measuring the adhesion of brittle films to ductile substrates with application to diamond-coated titanium. *Journal of Materials Research* **12**(7), 1900–1910.

Volinsky, A.A., Vella, J.B. and Gerberich, W.W. (2002a). *Thin Solid Films* **429**(1-2), 201–210.

Volinsky, A.A. Moody, N.R. and Gerberich, W.W. (2002b). *Acta Materalia* **50**(3), 441–466.

Weihs, T.P. Hong, S. Bravman, J.C. and Nix W. D. (1998). *Journal of Materials Research* **3**(5), 931–942.

Xia, Z.C. and Hutchinson, J.W. (2000). Crack patterns in thin films. *Journal of Mechanics and Physics of Solids* **48**, 1119.